



## BUOYANCY-DRIVEN MICROCLIMATE PHENOMENA: RANS, LES AND HYBRID MODELLING

Kemal Hanjalić<sup>1\*</sup>, Michael Hrebtov<sup>2</sup>, Saša Kenjereš<sup>1</sup>

<sup>1</sup>Department of Chemical Engineering, Delft University of Technology, The Netherlands

<sup>2</sup> Kutateladze Institute of Thermophysics SB RAS, Russia

### ABSTRACT

Thermal buoyancy is one of the key factors that govern local microclimate especially over terrains encompassing natural or man-made heat or cold islands. Thermal effects are particularly dominant in urban settlements in warm climate featured by prolonged summer heat waves, but also in temperate areas notably during winter windless episodes capped by inversion when buoyancy acts as the only driving force of local air movement and pollutants dispersion. Eye-catching orderly patterns such as vertically spiralling moisture columns and undulating fog patterns observed over lakes and large rivers at elevated surface temperature arouse public and research curiosity, but the understanding of the underlying physics and identifying the effects of such events on the human comfort and local air quality still pose a challenge. This paper provides a brief review of the current strategies in computer simulation and modelling of buoyancy-driven microclimate phenomena. The niches and limitations of the large-eddy simulations (LES) are briefly discussed and then the focus is turned to the Reynolds-averaged Navier–Stokes (RANS) methods currently prevailing as the most rational approach for predicting microclimate over realistic terrains and urban canopies. A time-resolved ensemble-averaged (T-RANS) three-equation algebraic stress/flux model (ASFM  $k-\varepsilon-\theta^2$ ) with the novel buoyancy-accounting functions for the ground boundary conditions, validated in a range of generic and engineering buoyant flows, is shown to reproduce the orderly structures observed over a real urban terrain with a large river acting as a strong localized source of heat and moisture. The model was subsequently applied to study the river-induced seasonal variation of the traffic-emitted CO distribution over the same city showing acceptable agreement with the field measurements. The paper closes with a short discussion of hybrid T-RANS/LES approaches in which the same or other RANS model is used only in the inner boundary layer on the ground and along the walls of urban buildings whereas the outer flow is entrusted to LES.

### 1. INTRODUCTION

Atmospheric boundary layers often display interesting natural phenomena in forms of large-scale self-organized flow structures of orderly shapes and morphology distinct from the usually indiscernible chaotic meteorological air movement in their background. Tropical cyclones - hurricanes and tornadoes - are the best known and most studied events of that kind because of their size, strength and devastating effects on the environment. However, similar though weaker phenomena are also observed, especially over large rivers and lakes or flat ground terrains at elevated surface temperature, in form of upward spiralling columnar structures, some topped by vortex rings. They become visible to observant by the entrained dust or vapour content, hence known as ‘dust devils’ and ‘steam devils’. Other orderly structures are the irregular hexagonal sheet-like thermal plumes on water surfaces warmer than the surrounding air, or undulating fog patterns observed along large rivers, Fig. 1. Their orderliness and specific shapes have long been arousing scientific curiosity. However, more importantly, these structures are also known to influence the local microclimate and human comfort through adverse effects in terms of localised wind and uncomfortable ambient air velocity, temperature and humidity, as well as local accumulation of air pollutants, thus affecting directly the local environmental quality. Densely populated cities with heavy road traffic and other emission sources, especially if situated in valleys with weak natural ventilation, are prone to pollutant accumulation during episodes of unfavourable weather conditions. In such situations, the morphology of the built objects may feedback the naturally formed orderly flow structures and further affect the local patterns of pollution dispersion.

\*Corresponding Author: khanjalic@gmail.com



**Figure 1:** Winter seen of the river Yenisei in Krasnoyarsk, Russia. *Left:* Morning mist with irregular honeycomb cellular patterns of sheet-like surface plumes (courtesy A. Gavrilov, November 2015). *Right:* a wavy fog pattern and upward spiralling vapour column ('steam devil') [courtesy of V. Raskalov (high resolution photos are available at <http://raskalov-vit.livejournal.com/122977.html>)].

The quest for better control and management of air quality in urban environment has brought the buoyancy-driven microclimate processes into the focus of the environmental research. Because of the physical complexity of the phenomena - intrinsic unsteadiness, large spatial scales, dominant self-organisation of specific flow structures, and others, computer simulations complemented by systematic field measurements are seen as the most viable method to provide the range of necessary information. However, the proper numerical modelling and simulations of spatial and temporal evolutions of flow, temperature and concentration fields in complex city-scale environment is a challenging task (Britter & Hanna [1], Hanjalić & Kenjereš [2]) which, can be accomplished by different simulation and modelling approaches.

All the phenomena mentioned could, in principle, be captured by direct and large-eddy simulations (DNS, LES). However, very high Rayleigh (Ra) number,  $\mathcal{O}(10^{16}-10^{20})$ , encountered in the lower atmosphere make it almost impossible to resolve *directly* the full turbulence spectrum with affordable numerical mesh. The main challenge is the resolving of the very thin hydrodynamic and especially the thermal boundary layer (a distance from the ground to the peak wind velocity and to the base of the mixed layer, respectively), which thicknesses decrease rapidly with an increase in the Ra number, roughly as  $\delta_\theta/H \propto Ra^{-1/3}$  and  $\delta_n/H \propto Ra^{-1/6}$ , resulting e.g. for  $Ra = 10^{18}$  in  $\delta_n/H \sim 10^{-3}$  and  $\delta_\theta/H \sim 10^{-6}$ , Fig 2. The LES have been reported to predict the atmospheric boundary layers in usually simplified configurations, but at the expense of large computational efforts using meshes with  $\mathcal{O}(10^7-10^9)$  cells (e.g. Nakanishi et al. [3], Rausch & Franke [4], Kenjereš & Hanjalić [5]). Moreover, complexity of the ground surface, diverse natural orography and man-made objects of versatile shapes and arrangement require sophisticated body-fitted numerical grid and long-time integration over at least several periods of the natural diurnal or other characteristic cycles. This generates enormous amount of data, the processing of which may require as much time and efforts as the computations. As remarked by Ehrenman [6] 'Having terabytes of data at our disposal greatly increases the chances that you will find the answer to even the toughest questions – if you don't mind searching for a needle in a giant digital haystack'.

Thus, for real-scales and configurations encountered in the environment, especially in urban ambient, the RANS modelling remains still the most viable approach, but the choice of the appropriate RANS model among many options is still an issue. Most popular RANS models use uncritically the linear eddy viscosity/diffusivity models (EVM/EDM) which have serious limitations when applied to thermal convection. Among other shortcomings, such models usually do not account for the buoyancy effects in EVM for the turbulent stress relating it directly to the mean-rate of strain. Moreover, the simple gradient diffusion hypothesis (SGDH) relates the turbulent heat flux directly to the aligned mean temperature gradient, which in buoyancy-driven flows is inappropriate. A case in point is a mixed layer in unstably stratified flow heated from below where intense mixing creates uniform temperature above the wall-adjacent layer, thus invalidating the common SGDH to model the dominant vertical heat flux.

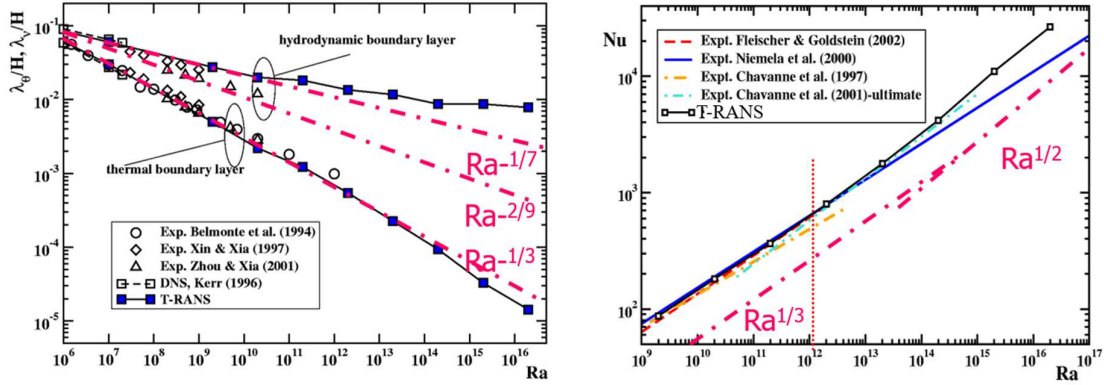


**Figure 2:** *Left:* Thicknesses of the hydrodynamic and thermal boundary layers. *Right:* Nu-Ra correlation for high Ra numbers. Symbols and dashed lines: experiments. Square symbols (left) and full lines: DNS and TRANS. Both figures indicates a change of the regime at  $Ra \sim 10^{12}$ . From Kenjereš & Hanjalić [10]

## 2. THE ‘T-RANS’ MODEL FOR HIGH Ra THERMAL CONVECTION

A way to decouple heat flux from the temperature gradient is to use an algebraic flux model obtained by truncation of the parent RANS differential equation for the turbulent heat flux while retaining all source terms, thus including the exact buoyancy term containing the temperature variance, and to solve a modelled transport equation for this variable. Another important aspect is the *mode* of solving the RANS equations. As already noted, buoyancy-driven flows are featured by inherent unsteadiness, energy non-equilibrium, counter-gradient diffusion, lack of universal scaling, all associated with distinct large-scale coherent flow structures acting as the major carriers of momentum and heat, but commonly regarded as intractable to steady RANS approach. However, treating the model equations as ensemble-averaged and solving in time (T-RANS<sup>1</sup>) with the RANS modelling accounting for the ‘subscale’, stochastic motion (akin to LES practice), was proved capable of reproducing the essentials of flow and heat transfer in a number of generic and real-scale configurations, Kenjereš & Hanjalić [7,8]. The ensemble-averaged equations for momentum, energy and species, denoted by  $\langle \rangle$ , are solved in the framework of a triple decomposition in which the instantaneous variable is split into a long-time-averaged, quasi-periodic (coherent) and stochastic fluctuation i.e.  $\hat{\Phi}(x_i, t) = \bar{\Phi}(x_i) + \varphi^c(x_i, t) + \varphi^s(x_i, t)$  so that the *effective* turbulent second moments are obtained as the sum of the deterministic (resolved, “apparent”) stress/flux and the modelled turbulence,  $\overline{\hat{\Phi}\hat{\Psi}} - \bar{\Phi}\bar{\Psi} = \overline{\varphi^c\varphi^c} + \overline{\varphi^s\varphi^s}$ .

The equations were closed with 3-equation algebraic RANS model (ASFM  $k-\varepsilon-\theta^2$ ) providing the turbulent stress, heat and mass fluxes for the unresolved (“subscale”) stochastic motion [7,8],

$$\langle u_i u_j \rangle = -\nu_t \underbrace{\left( \frac{\partial \langle U_i \rangle}{\partial x_j} + \frac{\partial \langle U_j \rangle}{\partial x_i} \right)}_{2S_j} + \frac{2}{3} \langle k \rangle \delta_{ij} - c_\phi \frac{\langle k \rangle}{\langle \varepsilon \rangle} \left[ \beta_T (g_i \langle \theta u_j \rangle + g_j \langle \theta u_i \rangle) \right] \quad (1)$$

$$\langle \theta u_i \rangle = -c_\phi \frac{\langle k \rangle}{\langle \varepsilon \rangle} \left( \langle u_i u_j \rangle \frac{\partial \langle T \rangle}{\partial x_j} + \xi \langle \theta u_j \rangle \frac{\partial \langle U_i \rangle}{\partial x_j} + \eta \beta_T g_i \langle \theta^2 \rangle \right) \quad (2)$$

<sup>1</sup> The T-RANS label implying Time-resolved (or Triple-decomposition) RANS was introduced by Kenjereš and Hanjalić [7] to distinguish this approach from the common unsteady RANS (URANS) applied to flows that are unsteady in the mean with timescale much longer than that for the turbulence.

$$\langle cu_i \rangle = -c_\phi \frac{\langle k \rangle}{\langle \varepsilon \rangle} \left( \langle u_i u_j \rangle \frac{\partial \langle C \rangle}{\partial x_j} + \xi \langle cu_j \rangle \frac{\partial \langle U_i \rangle}{\partial x_j} \right) \quad (3)$$

Equations (2) to (4) are closed by solving the transport equations for the turbulence kinetic energy  $\langle k \rangle$ , its dissipation rate  $\langle \varepsilon \rangle$  and the temperature variance  $\langle \theta^2 \rangle$ .

For complex real-scale flows, Eq (2) can be simplified to an EVM form with the buoyancy accounted through the flux Richardson number,  $R_f = -\mathcal{G}_k / \mathcal{P}_k$  (Apsley & Castro [11]).

$$\langle u_i u_j \rangle = \frac{2}{3} \langle k \rangle \delta_{ij} - \nu_i (1 - cR_f) 2S_{ij} \quad \text{where} \quad R_f = \frac{\mathcal{G}_k}{\mathcal{P}_k} \approx \frac{-\beta g \langle \theta w \rangle}{\langle uw \rangle (\partial \langle U \rangle / \partial z)}$$

where  $u$  and  $w$  denote fluctuating velocities in the horizontal  $x$  and vertical  $z$  directions respectively. Note that the above simplifications are derived by retaining *only* the vertical heat flux  $\langle \theta u_{i,j} \rangle \approx \langle \theta w \rangle$  and the horizontal shear  $S_{ij} \approx \partial \langle U \rangle / \partial z$ , and setting the prefactor of  $R_f$  equal to unity.

The ability of T-RANS to handle very high Ra, far beyond the present reach of LES is illustrated in Fig. 2 showing the Nusselt number obtained for Ra approaching  $10^{17}$ . At much lower Ra numbers the T-RANS results agree well with the available experiments and DNS data both for air ( $Pr=0.71$ ) and for mercury ( $Pr=0.025$ ) replicating the accepted dependence of Nusselt number on Ra,  $Nu \propto Ra^{1/3}$ . Moreover, the T-RANS results indicate a change in the regime at  $Ra \approx 10^{12}$  for  $Pr = \mathcal{O}(1)$  (apparently associated with the laminar to turbulent transition in the hydrodynamic wall boundary layer), and a trend towards Kraichnan's (1962) "ultimate" turbulence state characterized by the asymptotic solution  $Nu \propto Ra^{1/2}$  for Ra approaching infinity. The T-RANS computed thicknesses of the hydrodynamic and thermal wall boundary layer, shown in Fig. 2 (left), not only agree well with several experimental and DNS data for lower Ra numbers but also, Fig. 2 (right), show a steepening slope of the Nu dependency from  $Ra \approx 10^{13}$ , arguably supporting Kraichnan's proposal.

Further quantitative validations are provided in Fig. 3, which compares the T-RANS computed mean temperature with experiments and LES for  $Ra=10^5 - 10^{16}$  (left) and the breakdown between the resolved and stochastic (modelled) contributions to the vertical heat flux for a  $Ra=10^9$  (right). The total turbulent heat flux thus computed agrees well with the LES and also with a hybrid RANS/LES approach.

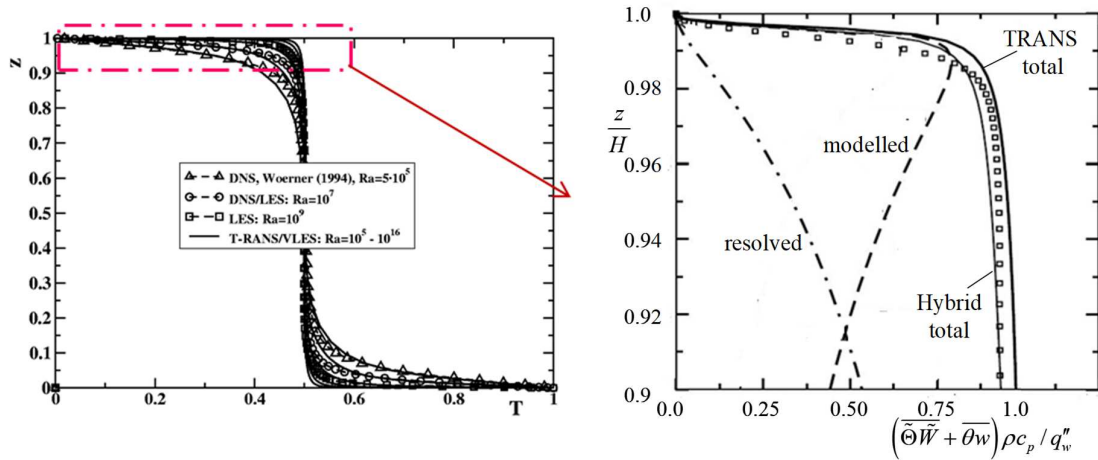


**Figure 3:** Validation of T-RANS WIN against DNS and LES in Rayleigh-Bénard convection. *Left:* long-term averaged fluid temperature at various Ra numbers; *Right:* vertical turbulent heat flux (modelled, resolved and total: for a range of Ra numbers. From Kenjereš & Hanjalić [5,7].

As shown below, the T-RANS has also been approved qualitatively by its ability to reproduce orderly organised phenomena observed in the nature. Figure 4 compares the hexagonal cell pattern of the sheet-like thermal plumes (or their remnants) on a frozen water surface with a T-RANS simulations of Rayleigh-Bénard (R-B) convection in an open-side domain  $4 \times 4 \times 1$  at  $Ra=10^9$  showing a remarkable qualitative similarity with observations despite using a coarse grid of  $82 \times 82 \times 72$  cells, admittedly clustered close to the wall. Such patterns are well reproduced by LES and DNS on much finer grids capturing, as expected, also much finer structures that are inaccessible to T-RANS on coarse meshes. However, the similarity of the organised structures and the successful reproduction of the Nu-Ra correlation by T-RANS (Fig. 2) confirms that small turbulence structures have little effects on the bulk flow properties and heat transfer.

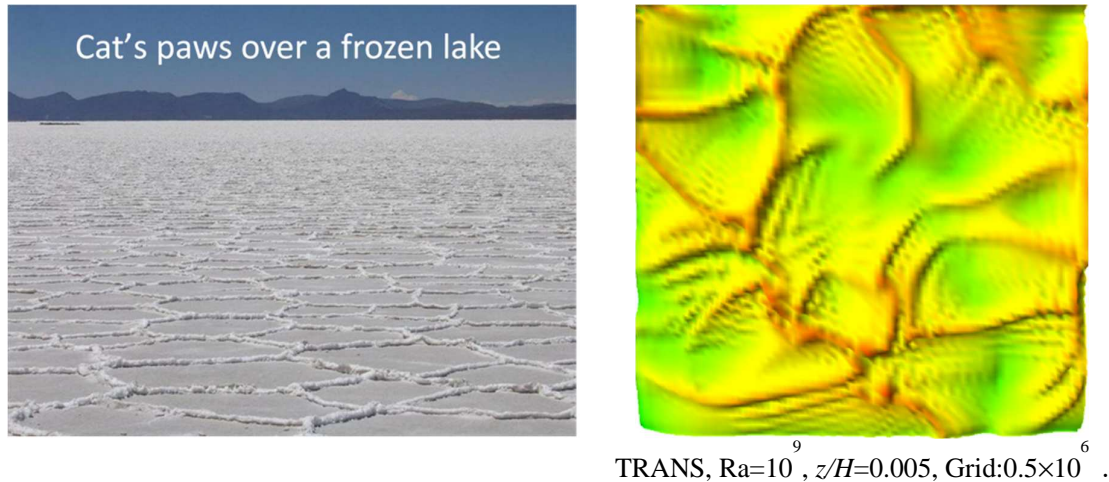


**Figure 4:** Irregular honeycomb cells of sheet-like plumes (or their remnants) in the nature (*left*) and their T-RANS simulations in R-B convection (*right*). From [9].

## 2.1 Buoyancy-accounting ground/wall boundary conditions

For real scale environmental situations, especially hilly terrains with urban and natural canopies, resolving the thin thermal and hydrodynamic ground/wall-adjacent layers (Figs. 2 and 3) with a sufficiently fine grid is not a viable option. Instead, the ground/wall boundary conditions have as a rule been handled by the wall-functions (WF) approach practiced in the computations of engineering flows. However, the standard WF do not account for buoyancy nor any non-equilibrium effects. Hanjalić and Hrebtov [12] proposed a generalised wall-functions formulation (GWF) of the boundary conditions for all mean and turbulence variables at the ground-adjacent grid nodes, well outside the molecular layer, suitable for high Ra numbers buoyancy dominated flows. The validation of the GWF with the algebraic stress/flux model (ASFM  $k-\varepsilon-\theta^2$ ) in the Rayleigh-Bénard (R-B) and penetrative convection of a mixed layer heated from below using one-dimensional and three dimensional grids of different density with 100 and only 20 nodes in the vertical directions, showed good agreements with the reference DNS/LES and experimental data even when using very coarse grid.

Figure 5 compares the mean temperature, vertical turbulent heat-flux and time growth of the mixed later after the onset of heating for selected meshes, in good compliance with the experiments. The approach is deemed functional for simulations of atmospheric boundary layers and pollutant transport over realistic complex hilly terrain with heat islands, urban and natural canopies, for diurnal cycles, or subjected to other time and space variations in ground conditions and stratification.

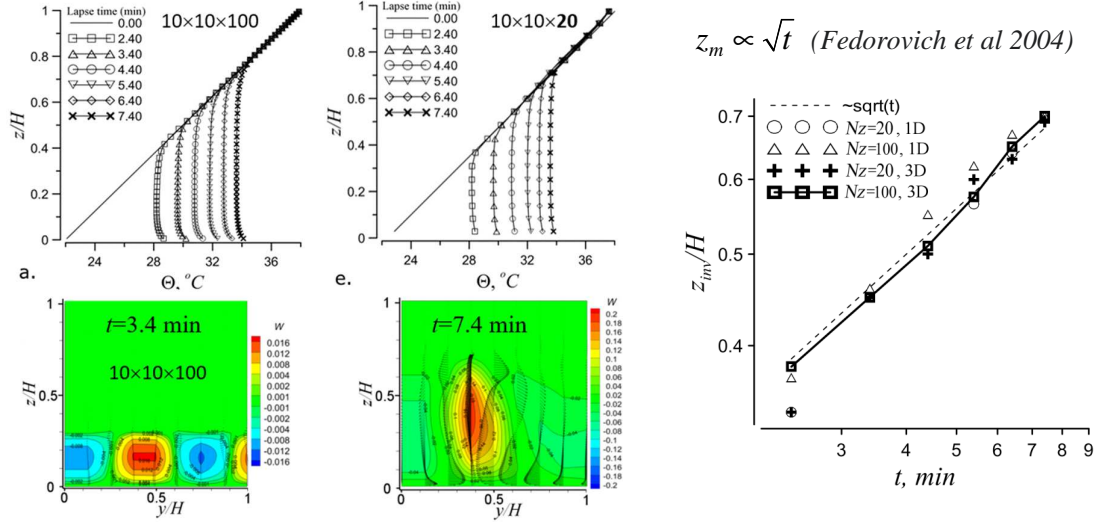


**Figure 5** Penetrative mixed layer heated from below *Left*: Short-time filtered ensemble-averaged T-RANS solutions for a fine and coarse mesh (*top*) and plane projections of velocity vectors superimposed on the coloured contours of the vertical velocity, for selected lapse times and domains (*bottom*). *Right*: Time evolution of the mixed-layer height (location of the maximum negative heat flux). From Hanjalić & Hrebtov, [12].

### 3. WINTER DIURNAL CONVECTION OVER REAL URBAN TERRAINS

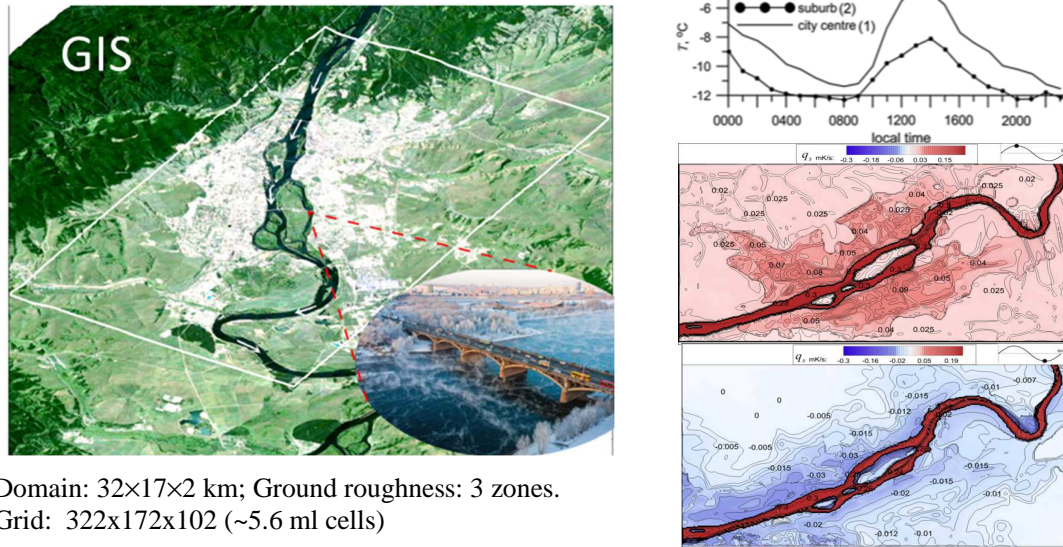
#### 3.1 City of Krasnoyarsk, Russia, with non-freezing river Yenisey

To illustrate the potential of the T-RANS+GFW approach for simulating real-life microclimate, we present briefly two cases of windless diurnal cycles in a weakly stratified atmospheric boundary layer over real urban orography topped by thermal inversion. The first case mimics the real winter environment of the city of Krasnoyarsk in Russia where the non-freezing river Yenisei (downstream from a hydropower water reservoir) acts as a thermal and moisture source. The river width is close to 1 km at its widest part, comparable with the inversion height. In such situations some rare natural microclimate phenomena have been observed, featuring an undulating fog pattern along the river accompanied by scattered spiralling columnar structures (‘steam devils’) topped by vortex rings. An idealized full diurnal cycle was simulated over a domain of  $32 \text{ km} \times 17 \text{ km} \times 2 \text{ km}$  meshed with a  $322 \times 172 \times 102$  grid (Hrebtov & Hanjalić [13]).

A realistic ground topography was generated from the Geographic Information System (GIS) data, Fig. 6 left. To account for the running river surface, a precursor simulation was conducted on a 2D finer mesh to compute the free-surface water velocity, used as the boundary conditions. The on-site temperature measurements at 2m above the ground for two weather stations showed the strength of the heat-island effect of about  $3^\circ\text{C}$  at its peak on windless days in winter. The spatial distribution of the ground temperature was estimated from the diurnal cycle of human activity and traffic intensity, accounting for building density and the main industrial facilities. The resulting normalised distribution was used to estimate the urban heat-island temperature, Fig. 6 right.

The reference potential temperature was specified from precursor simulations of the evolution of the mixed layer over uniformly heated ground into a stably stratified environment with a lapse rate of  $4^\circ\text{C}/\text{km}$  until it reached the targeted inversion base at a height of 1 km. The temperature above the inversion layer (at 1.6 km) was assumed to be  $-3^\circ\text{C}$ . A generic, uniform, sinusoidal, diurnal temperature cycle (marginally different from the measured one) was set for the ground ranging from  $-6^\circ\text{C}$  to  $-4^\circ\text{C}$ . In the city area a heat-island temperature variation was added with amplitude of  $2^\circ\text{C}$ . The coldest point in the diurnal cycle corresponds to 06:00 and the warmest to 18:00. The temperature of the river water

was assumed equal to 0 °C. The ground and the river were treated as rough surfaces defined in terms of the equivalent roughness for the city centre, the surrounding scarcely populated area, and the river.



Domain: 32×17×2 km; Ground roughness: 3 zones.  
Grid: 322×172×102 (~5.6 ml cells)

**Figure 6** Left: GIS view of Krasnoyarsk. Right: Measured ground temperature diurnal variations at two stations (top). Ground heat flux at noon (middle) and midnight (bottom). From Hrebtov & Hanjalić, [13])

Due to strong variation of the ground conditions over the surface and in time, the local air properties vary much from one location to another. With the periodic boundary conditions, evaluating the resolved properties requires first to compute the diurnal phase averaged values at a point over a number of cycles, an option that in atmospheric flows is neither practical nor realistic. Still, an estimate of the phase-averaged (“mean”) and the resolved properties can be obtained from spatial averaging over a limited area around the point considered by assuming local homogeneity in the horizontal planes. Figure 7 gives an impression of the local distribution of the mean temperature and vertical heat flux at selected locations (including the river) for three characteristic phase instants, averaged over a local 1 km×1 km area.

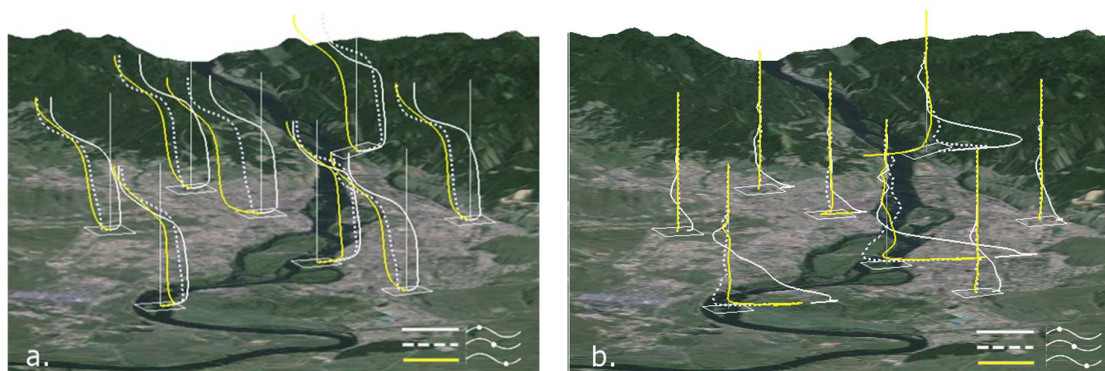


**Figure 7.** Temperature (a) and heat flux (b) profiles integrated over a local 1×1 km area at the three characteristic diurnal phases (noon, sunset and midnight), [13]

The strong heat transfer from the river throughout the whole diurnal cycle creates the main plumes over the river that govern the air movement over the whole area. During the night phase the river is virtually the only source of heat and the air motion is most intense around the river. Over that period

(Fig. 8, left) the largest convective structures appear in the form of a pair of long, counter-rotating convective rolls with axes aligned with the river, especially evident in the straightest section of the river. Moreover, a number of concentrated vortices and vortex rings are clearly visible along the river, superimposed on the two main river-parallel rolls. Far enough from the river (though still above the city) the air is stagnant. In the morning the solar irradiation and the increasing human activity begin to heat the nearby ground generating convective motion. As the heating progresses these rolls grow and begin to interact, intensifying the vertical heat transfer and reinforcing the creation of new plumes. The non-uniform ground heat flux and the warming of the air above within the ground layer creates a horizontal temperature gradient towards the river, which interacts with the gravitational vector acting as a baroclinic source of vorticity,  $\nabla(\beta T) \times \mathbf{g}$ , with its axes normal to  $\nabla T$ . In turn, this generates air movement in the direction of the gradient, entraining air from the suburbs toward the river and then into the plume rising above the warm water surface. The inversion layer acts as a barrier to the vertical motion, turning the flow and inducing horizontal spreading of the warm air away from the river at higher altitudes, thus creating a horizontal circulation to and away from the river, as shown by velocity vectors on planes normal to the river in Fig. 9.

The horizontal temperature gradient and the flow towards and away from the river interacting with shear and buoyancy can also be linked with the horizontal, counter-rotating roll pairs normal to the river over the city terrain. These are especially evident at peak heating (Fig. 8, right), though disappearing at night (Fig. 8, left). The width of the lineal vortex pairs is largest around and above the river, but their diameter, vorticity and intensity reduce with distance from the heat source (the river); hence their specific ‘trumpet’ or ‘carrot’ like shapes, with roots pointing outward from the river. The pattern is well reflected in the temperature and humidity distributions, especially at low elevations, as shown in Fig. 9.

The interaction of distinct large-scale vortex systems results in interesting phenomena such as wavy pattern of moisture plumes over the river and a chain of swirling columns topped by toroidal rings along the river, Fig. 10. A bird’s-eye view of the vortex structure over the terrain at two different times in the diurnal cycle shown in Fig.8 reveals such concentrated vertical vortex columns as well as vortex rings superimposed on the two main river-parallel rolls in the horizontal plane at higher elevations. This is in particular visible at peak cooling when the river-normal ‘trumpet’ vortices are absent, Fig. 8 left.

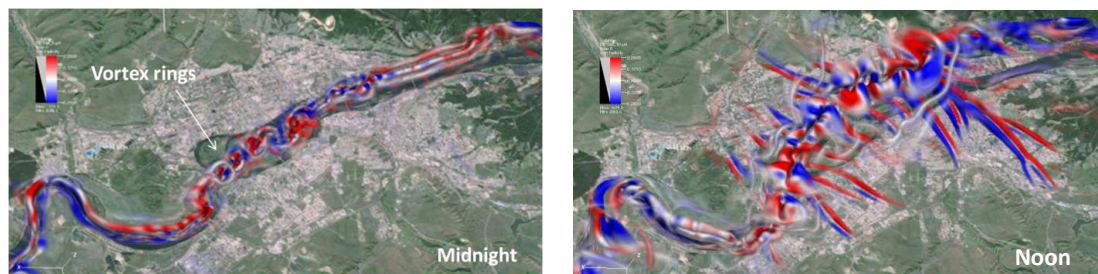


**Figure 8.** Vortical structure at extreme phases visualized by the  $Q$  criterion, coloured by helicity ( $\omega_i u_i$ ), [13].

The concentrated vertical vortex columns, believed to be the precursors of the swirling ‘steam devils’, [4] are initiated by the interaction of some of the opposing river-normal longitudinal rolls over the river surface, creating another distinct vortex system in the form of concentrated vertically-oriented counter-rotating vortices on and around the river. The toroidal rings on the top of swirling columns, however, seem to be created by a roll-up instability in the vertical shear layers around the edge and near the top of the columnar plume beneath the inversion layer. Presumably, they are also affected by shear at the moving water surface, which seems to be the prevailing mechanism during the night when the river plume is weak. As illustrated in Fig 10 (right), the T-RANS computation reported in [13] reproduced the overall shape and swirling pattern of the columnar structures, closely resembling their natural appearance, Fig. 10.

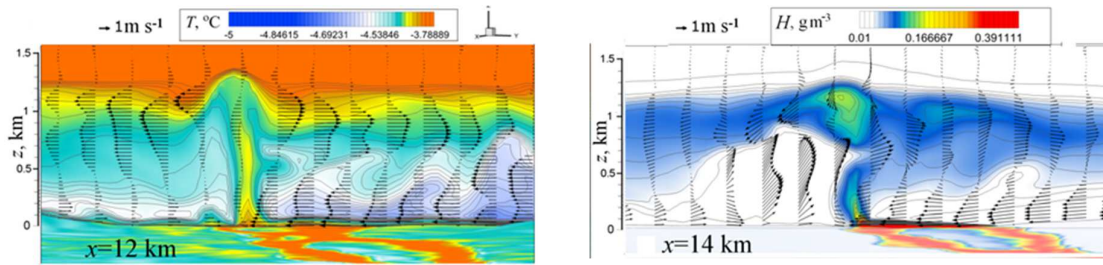


**Figure 9** Horizontal velocity vector projections with temperature (*left*) and water vapour concentration (*right*) in selected river-normal vertical cross-sections at 18:00 LT. Note the river and local terrain at the bottom coloured with the same colour bars, [13].

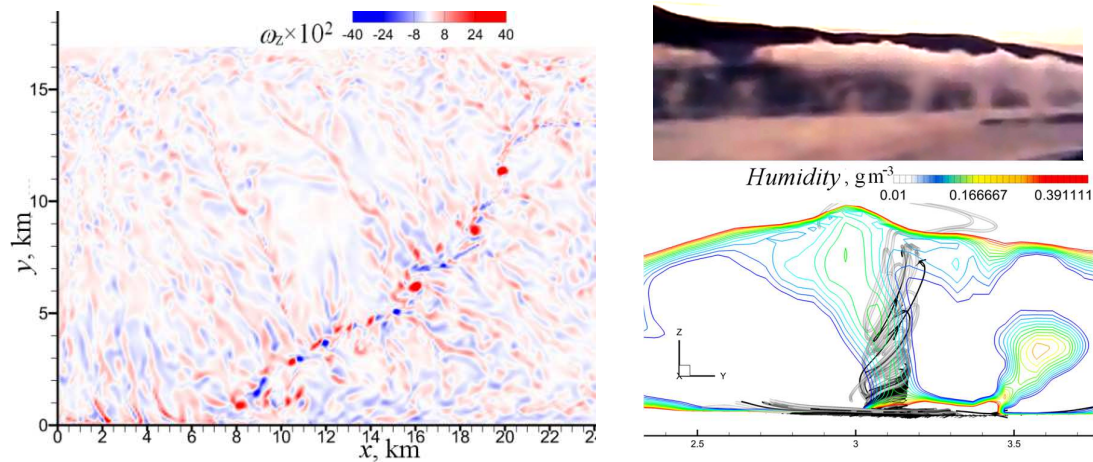


**Figure 10** *Left*: Vertical vorticity at 20 m altitude along the river. *Right*: Observed (*top*) and computed (*bottom*) spiralling columnar structures at 12.00 hr, [https://youtu.be/hWOP3u\\_m9xQ](https://youtu.be/hWOP3u_m9xQ). [13].

We close this section with a short discussion of possible micro-climate impacts on pollution in the urban environment. A case in point is the seasonal variation of carbon monoxide (CO) levels in winter and summer observed at different locations around the City of Krasnoyarsk despite a fairly similar emission from road traffic throughout the year. The T-RANS simulations reported by Hrebtov and Hanjalić [14] captured reasonably well the major recorded differences in CO concentrations between winter and summer conditions, indicating that the origin of the anomaly can be attributed to a different role of the river on the local microclimate, acting as heat source or heat sink depending on the season. The instantaneous snapshots of volume rendering of the CO concentration at 18:00 in Fig. 10 (top) give an impression of a typical late afternoon pollutant dispersion over the city in summer (left) and winter (right). The grey-scales in the two figures ranging from full transparency for zero concentration to full opacity for its maximum, differ in absolute values but they both show the maximum concentration in the same central downtown region, though with a markedly different distributions.

Systematic validations of computer simulation of real-scale atmospheric processes are usually limited due to the scarcity of reference data. However, averaged ground-level measurements are available at particular points of the city of Krasnoyarsk that show the difference between the summer and winter pollutant concentration distribution (Mikhailuta et al.[15]). To provide at least some quantitative justification, Fig. 11 (bottom) shows a comparison of the measured [15] and computed daily averaged CO concentration in summer and winter at a number of locations scattered over the city area (Fig. 1 in [14]). In Fig. 11, the measuring stations are sequenced (from left to right) to show a monotonic increase in the measured concentration (apart from the last two locations), and thus to provide

an impression of the CO variation over the city. Despite some noted differences in the absolute values of the measured and simulated data, the agreement can be considered as satisfactory.

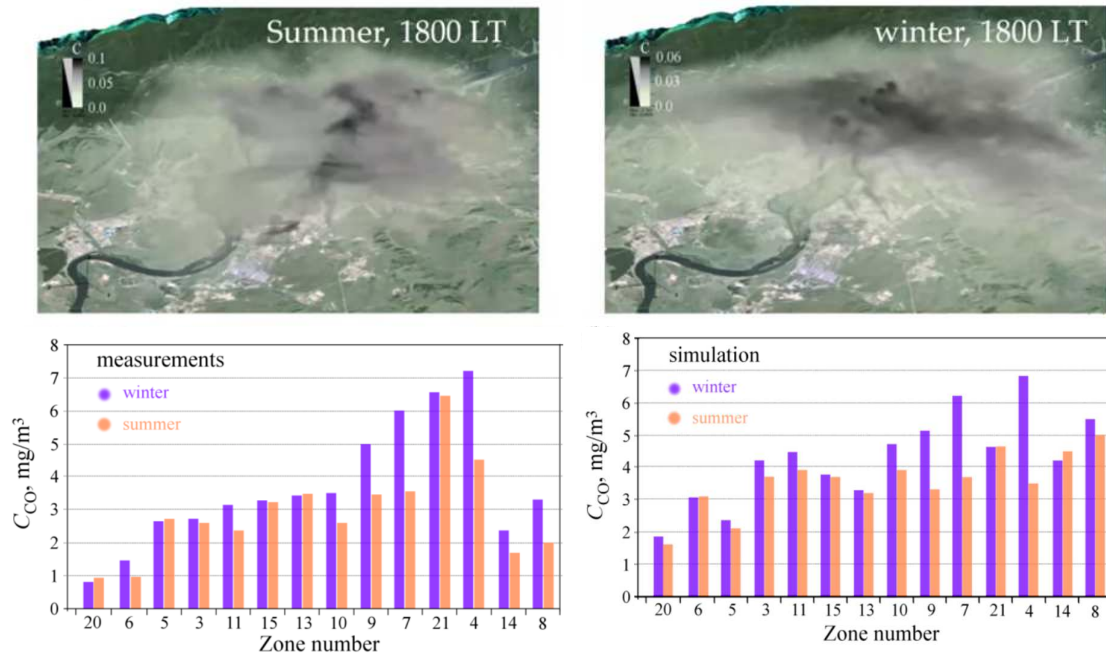


**Figure 11.** Seasonal variation of traffic-emitted CO distribution over Krasnoyarsk. *Top:* Instantaneous CO concentration at 1800 LT in the summer (left) and winter (right). *Bottom:* measured and simulated CO at 10 m altitude (averaged over a day) at various locations in the city). Blue: winter; orange: summer. [14].

The computational data show the same trend as the measurements, both for winter and summer, qualitatively exposing the difference between the two seasons. The maximum seasonal differences in the mean CO concentration were observed at points 4, 7, 9 and 10 located close to the river banks where as expected, the change in the air circulation pattern between the summer and winter is strongest. The simulated seasonal differences in the absolute concentration values for the mentioned points are markedly similar to the measurements. This leads to the conclusion that the river thermal effect (acting as a heat island) is indeed strong enough to be the prime cause of the observed seasonal variation.

Despite some differences in the absolute values of CO concentration at some locations, in view of some unavoidable ambivalence in the input data and boundary conditions, as well as some uncertainties in the measurements, the considered example confirms that the applied T-RANS modelling approach can serve as an acceptable tool for providing insight into the effects of microclimate on the pollution dispersion.

### 3.2 The valley and downtown of Sarajevo

In the case of Krasnoyarsk discussed above with the focus on the role and effects of a large river acting as a localised heat island, the urban structures were not treated explicitly but their effects were modelled by areal representations of the equivalent surface roughness and ground temperature. A different challenge is encountered if one considers the real urban morphology with a realistic replica of a variety of building shapes and arrangements, their thermal properties and heat exchange with the environment, which may require specific upgrades of the turbulence model or the simulation approach itself. To give a flavour of such a challenge, we present some excerpts of simulations of a diurnal cycle in the valley

and city of Sarajevo during winter windless- and mild-easterly wind episodes capped by inversion with the same T-RANS model. Two subcases are considered: first, a mesoscale domain of  $18.5 \times 12.5 \times 3$  km, meshed with 4.6 mill cells, encompassing the whole valley with the surrounding slopes in which the building structures were modelled as a surface of equivalent roughness with a sinusoidal time- and area distribution of the surface temperature, corresponding to peak  $Ra=4.2 \times 10^{17}$ . A view of the valley with thermal plumes coloured by vertical velocity at noon is shown in Fig 12 left (Kenjereš et al. [16]).

In the second subcase, considered was a segment of the downtown of  $1.75 \times 0.75 \times 0.2$  km replicating from the GIS data the real shapes and arrangement of all larger buildings and high-rise towers. The domain was discretized with a non-uniform buildings-resolving mesh (down to 3.5m) with  $614 \times 322 \times 52 = 10.3$  mil cells, clustered around the emission sources and zones with high buildings density where air velocity is expected to be low and thus prone to trapping and aggregating the pollutants. Starting with a stably stratified linear reference vertical temperature distribution with a lapse rate of 4 K/km, the domain was subjected to the same diurnal variation of the ground- and buildings outside walls temperature as in the previous subcase, now complemented with a mild easterly wind of 0.5 m/s.

An impression of the early winter morning picture of air flow and pollutant concentration in the downtown is given in Fig. 12 right illustrating the extent of simulation-provided details of spatial and temporal evolution of flow and scalar fields over the city. It is noted that, at least at zero or low wind, the air flow field is highly sensitive to the thermal buoyancy, showing notable modifications soon after the onset of ground heating even by a fraction of degree above the surrounding ambient.

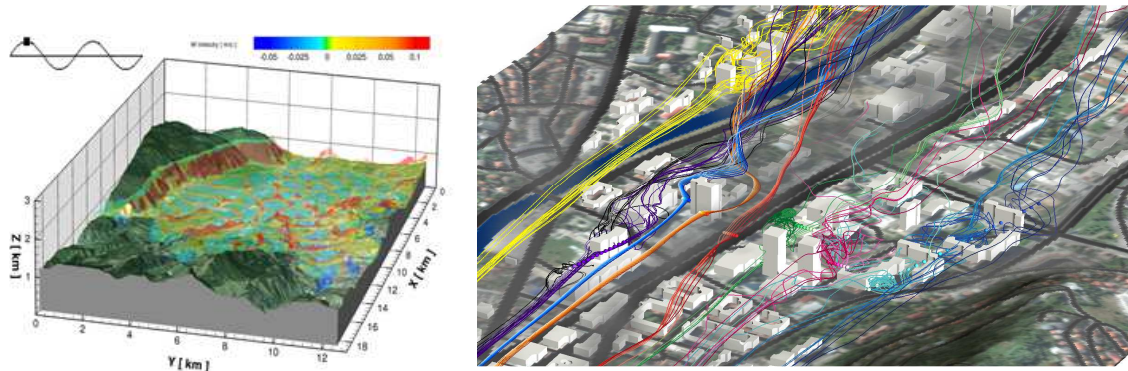


**Figure 12.** *Left:* Thermal plumes at noon in Sarajevo Valley, colored by vertical velocity. *Right:* Early morning (8:00 hr) in the downtown during winter thermal inversion and mild easterly wind - pollutant concentration represented by semi-translucent fog. Blue, purple and black streamlines deflections from the wind direction due to buildings and heat island. From Kenjeres et al. [16]

#### 4. CONCLUDING REMARKS AND OUTLOOK

Just as in general CFD, two mainstream strategies prevail in the computation of geophysical flows: the (U)RANS and LES, with surprisingly few Hybrid methods if any. Unlike in engineering and industry, the LES seems to have been the preferred option among the geophysics community, especially in atmospheric sciences (“Turbulence models cannot serve as a predictive tool” (?), Wyngaard, 1992). But most publications on LES deal with atmospheric boundary layers (ABL) over flat terrains in micro- and mesoscale domains,  $\mathcal{O}(10-100)$  km, using very fine meshes with  $10^8-10^9$  cells with the Monin-Obukhov scaling for the ground conditions. However, the increasing interest in real orography, natural and urban (built) canopies requiring boundary-fitted clustered meshes (a formidable computational burden on LES), has been reviving attention to the more practical and economical URANS approach that offers more flexibility, especially when the mitigation of air pollution is in focus.

The here presented time-resolved ensemble-averaged (T-RANS) three-equation algebraic stress/flux (ASFM  $k-\varepsilon-\theta^2$ ) and similar models with the novel buoyancy-accounting functions for the ground boundary conditions, is seen, at least at present, as a more rational option to LES. The model is shown capable of reproducing some real microclimate phenomena governed by large-scale orderly flow structures in accord with observations in the nature. Together with some (admittedly limited) field measurements, the results provide sufficient confidence in the model predictive capability for the microclimate dynamics including pollutant dispersion in real environmental situations with the authentic terrain complexity and the meteorological conditions.

For the application to real urban morphology encompassing buildings of a variety of shapes and arrangement, a blending of the present or similar RANS model with LES in a hybrid mode, currently under investigation, is seen as the next step forward in improving the T-RANS approach for modelling real complex urban environment.

And, as a final remark, we note that the here presented findings and conclusions apply equally to engineering and industrial flows in complex settings driven or affected by thermal buoyancy (natural and mixed convection) at high Rayleigh numbers.

## REFERENCES

- [1] R.E. Britter & S.R. Hanna, Flow and dispersion in urban areas, *Annu. Rev. Fluid Mech.* **35** (2003) 469–96
- [2] K. Hanjalić & S. Kenjereš, Dynamic simulation of pollutant dispersion over complex urban terrains: a tool for sustainable development, control and management”, *Energy* **30** (2005) 1481-1497.
- [3] M. Nakanishi, R. Shibuya, J. It & H. Niino, Large-eddy simulation of a Residual Layer: low-level jet, convective rolls, and Kelvin–Helmholtz instability, *J. Atmos. Sci.* **71** (2014) 4473-4491.
- [4] S. Raasch, & T. Franke, Structure and formation of dust devil-like vortices in the atmospheric boundary layer: A high-resolution numerical study, *J. Geophys. Res.*, **116** (2011) D16120.
- [5] S. Kenjereš and K. Hanjalić, LES, T-RANS and hybrid simulations of thermal convection at high Ra number, *Int. J. Heat & Fluid Flow* **27** (2006) 800-810.
- [6] G. Ehrenman, Mining what others miss. *Mech. Eng. (ASME)* **127/2** (2005), 26–31.
- [7] S. Kenjereš, S. & K. Hanjalić, Transient analysis of Rayleigh–Bénard convection with a RANS model, *Int. J. Heat & Fluid Flow* **20** (1999) 329-340.
- [8] S. Kenjereš & K. Hanjalić, Combined effects of terrain orography and thermal stratification on pollutant dispersion in a town valley: a T-RANS simulation, *J. Turbulence*, **26** (2002) 1-25.
- [9] S. Kenjereš & K. Hanjalić, A numerical insight into flow structure in ultra-turbulent thermal convection, *Phys. Rev. E* **66** (3), Art.No.036307, Part 2B (2002), 1-5.
- [10] S. Kenjereš & K. Hanjalić, Tackling complex turbulent flows with Transient RANS, *Fluid Dyn. Res.* **41**, 012201 (2009) 1-32.
- [11] D. D. Apsley & I. P. Castro, A limited-length-scale  $k-\varepsilon$  model for the neutral and stably-stratified atmospheric boundary layer, *Bound. Layer Meteorol.* **83** (1997) 75–98.
- [12] K. Hanjalić, K. and Hrebtov M. 2016, Ground boundary conditions for thermal convection over horizontal surfaces at high Rayleigh numbers. *Bound. Layer Meteorol.* **160**(1), 41-61.
- [13] M. Hrebtov & K. Hanjalić, Numerical study of winter diurnal convection over the city of Krasnoyarsk: effects of non-freezing river, undulating fog and steam devils, *Bound. Layer Meteorol.* **3**, (2017)469–495.
- [14] M. Hrebtov & K. Hanjalić, River-induced anomalies in seasonal variation of traffic-emitted CO distribution over the City of Krasnoyarsk, *Atmosphere* **10** (7) (2019) 407 (1-20).
- [15] S.V. Mikhailuta, O.v. Taseiko, A. Pitt, A.A. Lezhenin, Y.V. Zakharov, Seasonal variations of air pollutant concentrations within Krasnoyarsk City. *Environ. Monit. Assess.*, **149** (2009), 329–341.
- [16] S. Kenjereš, A. Bevrnja, A. Žilić & K. Hanjalić, Modelling pollutant dispersion over a city in a hilly terrain under initially stable and neutral stratification, In K. Hanjalić et al. eds, *Turbulence, Heat and Mass Transfer* 8, Begell House Inc. (2015) pp.719-722, New York.